A comparative study of pilot-based channel estimators for wireless OFDM

Sandell, Magnus; Edfors, Ove

1996

A comparative study of pilot-based channel estimators for wireless OFDM

Magnus Sandell and Ove Edfors

September 1996

Abstract

This report deals with pilot-based channel estimation in wireless OFDM systems. We assume that the receiver is able to use all transmitted pilots, which is the case in broadcasting and in the downlink of a multiuser system. Four estimators (of which two have been proposed in the literature) are compared, both in terms of mean-squared error and bit-error rates. In the latter case, we simulate a multiuser system which incorporates channel coding. The channel estimation is a two-dimensional problem (time and frequency), and both separable and non-separable estimators are investigated. We design low-rank approximations of these estimators, and compare the performance at given complexities. The comparison shows that the use of separable estimators increases the performance substantially, compared to non-separable estimators with the same complexity. For the scenario investigated in this report the performance is further improved by applying low-rank approximations separable estimators.

Chapter 1

Introduction

Wireless orthogonal frequency-division multiplexing (OFDM) is currently used and proposed for several broadcasting applications. The European standard for digital audio broadcast (DAB) [1] uses OFDM with differential phase-shift keying (DPSK). This is suitable for low bit-rate systems, but when higher bit-rates are required, multiamplitude modulation is more appropriate. Proposals for digital video broadcasting [2, 3] have included multiamplitude modulation OFDM. These schemes can be made differential, which offers the advantage of avoiding channel estimation. Differential amplitude and phase shift keying (DAPSK) [4] is an example of this approach. In DAPSK, however, the constellation points are non-uniformly distributed in the signal space, which reduces performance. There may also be metric difficulties concerning decoding. Coherent modulation, on the other hand, gives better performance, but because of the necessary channel estimation, it requires more complexity at the receiver. It is of interest, therefore, to investigate the performance of coherent OFDM systems using channel estimators with different levels of complexity. In this paper we analyze low-complexity coherent demodulation receiver schemes suitable for high bit-rate OFDM.

One way of estimating the channel in a flat fading environment is to multiplex pilots (known symbols) into the transmitted signal. From these symbols, all channel attenuations are estimated with an interpolation filter. This technique is called pilot-symbol assisted modulation (PSAM) and was introduced for single-carrier systems by Moher and Lodge [5] and analyzed by Cavers [6]. Since each subchannel in OFDM is flat fading, PSAM can be generalized to two dimensions where pilots are transmitted in certain positions in the time and frequency grid of OFDM. The channel estimation is then performed by a two-dimensional interpolation. Höher [7] proposes to use finite impulse response (FIR) filters for this and to separate the use of time- and frequency correlation. He argues that this is a good trade-off between complexity and performance.

The spacing of pilot symbols in PSAM for single-carrier systems was investigated in [6]. It was found that the optimum spacing was somewhat closer than the Nyquist rate, *i.e.*, the inverse of the bandwidth of the channel covariance function. We generalize this result to two dimensions for the OFDM time-frequency grid. Using a dense pilot pattern means that the channel is oversampled, implying that low-rank estimation methods [8] can work well. This type of low-complexity estimation projects the observations onto a subspace of smaller dimension and performs the estimation in that subspace. By over-

sampling the channel, *i.e.*, placing the pilot symbols close to each other, the observations essentially lie in a subspace and low-rank estimation is very effective.

In this report we present and analyze pilot-based OFDM channel estimators that rely on both time and frequency correlation of the fading channel. The estimators are linear and feedforward, *i.e.,* no decision direction or feedback is used. We divide them into two classes: 2-dimensional (2-D) and separable estimators. The latter uses 1-dimensional (1-D) interpolation filters in the time and frequency directions separately. In each class, we compare a FIR Wiener filter [9] with a low-rank approximation of the linear minimum mean-squared error (LMMSE) estimator [8]. The estimators are compared both in terms of mean-squared error (MSE) and coded bit-error rate (BER). The system and the scenario are introduced in Section 2. The estimators are described in Section 3 and their performance is presented in Section 4, both in terms of mean-squared error and coded bit-error rate. Finally, in Section 5 we present conclusions.

Chapter 2

System description

2.1 OFDM system

In this report we consider an OFDM system operating in a Rayleigh fading channel environment. This system uses a cyclic prefix [10], which is a copy of the last part of the OFDM symbol and acts as a guardspace between consecutive OFDM symbols. Hence, if the impulse response of the channel is shorter than the cyclic prefix, inter-symbol interference (ISI) is avoided. Furthermore, if the channel is assumed constant during one OFDM symbol, inter-carrier interference (ICI) is also avoided [10].

In Figure 2.1a a schematic view of the base-band OFDM system is shown. The mod-

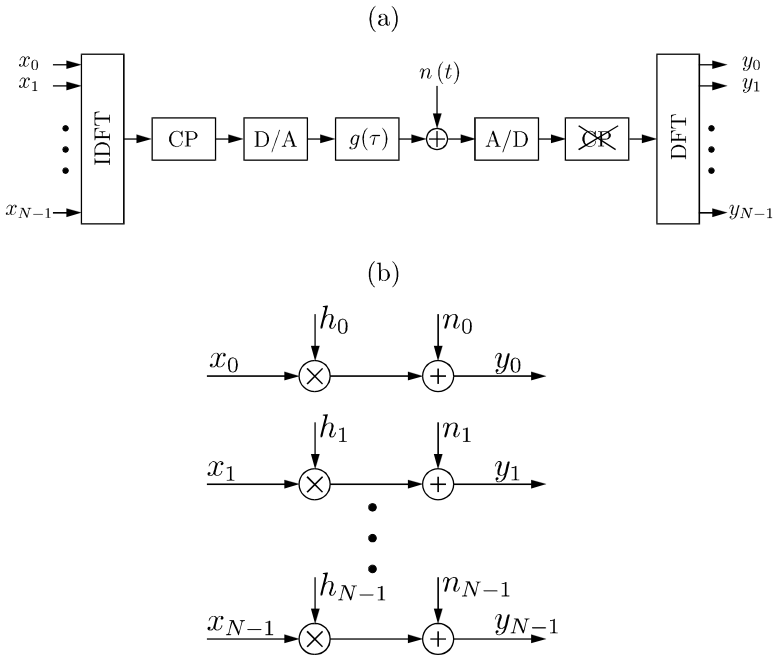

Figure 2.1: OFDM system. (a) Base-band model, (b) parallel subchannels model. 'CP' and '$\not$CP' denote the insertion and deletion of the cyclic prefix, respectively.

ulation on N subcarriers is performed by an inverse discrete Fourier transform (IDFT) in the transmitter [11]. Similarly, demodulation is done with a discrete Fourier transform (DFT) in the receiver. The effective symbol length is $T = NT_s$, where T_s is the sampling period of the system. Adding a cyclic prefix (CP) with a length of $T_G = LT_s$ makes the total symbol length $T + T_G$. If ISI and ICI are eliminated, we can describe the system as a set of parallel Gaussian channels [12], shown in Figure 2.1b, with correlated channel attenuations

$$h_k = G\left(\frac{k}{NT_s}\right), k = 0 \ldots N-1,$$

where $G(\cdot)$ is the frequency response of the channel $g(\tau)$ during the OFDM symbol. The received signal y_k on subchannel k can thus be described as

$$y_k = h_k x_k + n_k, \tag{2.1}$$

where x_k is the transmitted data symbol and n_k the channel noise at subcarrier k. The relation (2.1) holds for every OFDM symbol, thus creating a two-dimensional grid with frequency (subcarriers) on one axis and time (OFDM symbols) on the other.

2.2 Scenario

The channel estimation is based on pilots transmitted at certain positions in the time-frequency grid of the OFDM system. The channel attenuations are estimated by means of interpolation between these pilots, where we assume that the channel estimators can use all transmitted pilots. This is the case in, *e.g.*, broadcasting or in the downlink of a multiuser system. In both these cases there is only one physical channel between the transmitter and the receiver. Thus channel attenuations in neighboring time-frequency gridpoints are highly correlated, a feature that can be used for channel estimation. In the uplink of a multiuser system on the other hand, each user has their own physical channel, so channel attenuations stemming from different mobile transmitters must be assumed to be uncorrelated. To estimate the attenuations for one user, only pilots transmitted by that user can be used. Thus, the uplink is quite different from our scenario and will not be considered here.

The investigated OFDM system has a bandwidth of 5 MHz and is operating in the 2.2 GHz frequency band. The number of subcarriers is $N = 1024$, which makes the effective symbol length 205 μs. The environment is a macrocell which is assumed to have a maximum delay spread of 10 μs and a maximum Doppler frequency of 240 Hz. Thus, the maximum Doppler frequency relative to the inter-carrier spacing is $f_{D,\max} = 5$ %, which corresponds to a vehicle speed of 120 km/h. The power delay profile is exponentially decaying with root mean square (RMS) width $\tau_{\text{rms}} = 2.2\,\mu$s. To eliminate ISI, we use a guard space of 10 μs which corresponds to $L = 50$ samples. The length of the OFDM symbol is $205 + 10 = 215$ μs which makes the relative size of the guard space 5%. The corresponding SNR loss is 0.2 dB. Our system model assumes that the channel is constant during an OFDM symbol. In reality ICI occurs due to channel fading during the transmission of an OFDM symbol [13, 14]. However, with a maximum relative Doppler

frequency of 5%, the signal-to-ICI ratio is 24 dB [14]. This is negligible in the SNR ranges we are looking at, and consequently we ignore the ICI and use the model in (2.1).

Interleaving is performed separately in frequency and time over a frame consisting of 50 OFDM symbols. This corresponds to a maximum delay of 10.7 ms. First, interleaving in frequency is done by placing consecutive data symbols 64 subcarriers apart. Interleaving is then performed in time with a unique pattern for each subcarrier. These patterns are random permutations and changed every frame. By having different interleaving patterns on all subcarriers, channel attenuations are interleaved in both time and frequency. This produces an almost perfect interleaving with no significant performance loss.

For error correction, a rate 1/2 convolutional code with the octal polynomials $(133, 171)$ is used, *i.e.,* the code polynomials are [15]

$$\begin{aligned} g_0^{(0)}(D) &= 1 + D + D^3 + D^4 + D^6 \\ g_0^{(1)}(D) &= 1 + D^3 + D^4 + D^5 + D^6. \end{aligned}$$

The constraint length is $n_E = 7$ and a tail of $n_E + 1 = 8$ zeros is appended to clear the encoder's memory. The receiver uses a soft-decision Viterbi decoder with a truncated memory length of $5n_E = 35$ bits. The bits are modulated using BPSK in each dimension and the inphase and quadrature parts are concatenated to form QPSK symbols. This makes the data rate of the system 4.7 Mbit/s.

2.3 Channel model

In our analysis we use the wide-sense stationary uncorrelated scattering (WSSUS) channel model introduced in [16]. By considering the channel to be constant over one OFDM symbol, the instantaneous frequency response of the $M-$path channel at time t is

$$G(f;t) = \frac{1}{\sqrt{M}} \sum_{n=1}^{M} e^{j(\theta_n + 2\pi F_{D_n} t - 2\pi f \tau_n)}, \tag{2.2}$$

where θ_n is the phase, F_{D_n} the Doppler frequency and τ_n the delay of the n^{th} path. All these parameters are independent random variables. To obtain Rayleigh fading with the Jakes' spectrum [17] and an exponentially decaying power delay profile with RMS-value τ_{rms}, we choose the probability density functions as [16]

$$\begin{aligned} p_\theta(\theta) &= 1/2\pi, & 0 \le \theta < 2\pi \\ p_{F_D}(F_D) &= \frac{1}{\pi F_{D,\max}\sqrt{1-\left(F_D/F_{D,\max}\right)^2}}, & |F_D| < F_{D,\max} \\ p_\tau(\tau) &= \frac{e^{-\tau/\tau_{\text{rms}}}}{\tau_{\text{rms}}\left(1-e^{-T_{cp}/\tau_{\text{rms}}}\right)}, & 0 \le \tau \le T_{cp} \end{aligned}.$$

The random variables F_D and τ can easily be obtained from a uniformly distributed random generator with outputs $\in [0, 1]$ by using the inverses of the desired cumulative distribution functions [16].

2.4 Pilot pattern

By using a two-dimensional generalization [7] of pilot-symbol assisted modulation [5], known symbols (pilots) are transmitted on certain positions in the time-frequency grid. The number of pilots to use is a trade-off between data rate and channel estimation performance. However, by viewing the channel estimation in the time-frequency grid as a two-dimensional interpolation, fundamental limits on the density of pilots can be derived. The scattered pilot symbols can be seen as (noisy) samples of the two-dimensional stochastic signal $G(f;t)$. These samples have to be placed close enough to fulfil the sampling theorem and avoid aliasing. Note that the effective SNR is lowered by using many pilots, since a smaller part of the transmitted power is used for data symbols. Since $G(f;t)$ in (2.2) is the Fourier transform of the channel impulse response at time t (which is assumed to be constant for one OFDM symbol), the auto-covariance function of $G(f;t)$ is the spaced-frequency, spaced-time correlation function ϕ_C of the channel [18]

$$R_{GG}\left(\Delta f, \Delta t\right) = E\left\{G(f;t)G^*(f-\Delta f;t-\Delta t)\right\} = \phi_C\left(\Delta f, \Delta t\right).$$

The bandwidth of this function is B_d (the Doppler spread) in the Δf direction and $\tau_{\max}$ (the multipath spread) in the Δt direction [18]. For the analyzed OFDM system we have

$$\begin{aligned} B_d &= 2F_{D,\max} = \frac{2f_{D,\max}}{NT_s} \\ \tau_{\max} &= LT_s, \end{aligned}$$

where $f_{D,\max}$ is the maximum Doppler frequency relative to the inter-carrier spacing.

If we assume that pilots are placed N_f subcarriers apart in every N_t OFDM symbols we have

$$h_{k,l} = G\left(k \cdot \frac{N_f}{NT_s}, l \cdot N_t\left(N+L\right)T_s\right)$$

since the inter-carrier spacing is $1/NT_s$ and the duration of an OFDM symbol is $(N+L)\,T_s$. To fulfill the sampling theorem [19] we need

$$\begin{aligned} N_f &< \frac{N}{L} \\ N_t &< \frac{1}{2\left(1+\frac{L}{N}\right)f_{D,\max}}. \end{aligned}$$

In the analyzed system we have $N = 1024$, $L = 50$ and $f_{D,\max} = 0.05$ which gives

$$\begin{aligned} N_f &< \frac{1024}{50} = 20.5 \\ N_t &< \frac{1}{2\left(1+\frac{50}{1024}\right)0.05} = 9.\,5. \end{aligned}$$

In [6], where PSAM for single-carrier systems is analyzed, it is shown that the BER can be lowered by placing the pilot symbols closer than that specified by the sampling theorem. Note that there exists a pilot spacing which optimizes the trade-off between

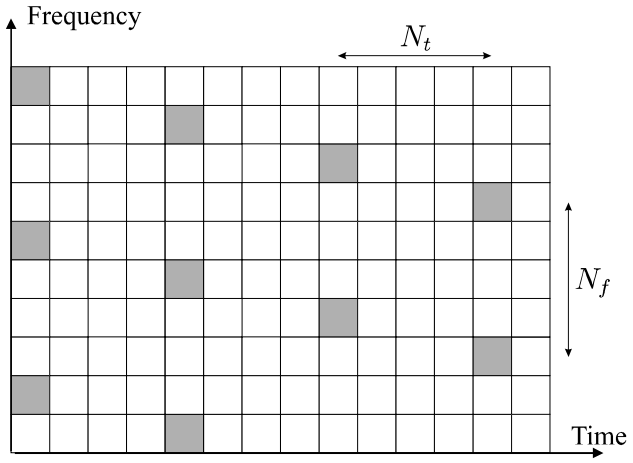

Figure 2.2: The pilot pattern used in the system. Pilot symbols are marked with grey squares.

improved channel estimation and reduced SNR on the data symbols. By varying the pilot spacings N_f and N_t, it was found that $N_f = 4$ and $N_t = 4$ was close to optimal in terms of BER. The used pilot pattern is shown in Figure 2.2. This means that 1/16 ($\approx 6\%$) of the bandwidth and the transmitted power is used for pilots. Note that the channel is oversampled which means that low-rank estimators can be very effective [8].

In our study the pilot symbols have the same average power as the data symbols. However a technique called boosted pilots can also be used, which is proposed for DVB [3]. This means that the pilot symbols are transmitted with a higher average power than the data symbols. The average SNR on the data symbols is reduced but the channel estimates are better since the SNR at the pilot symbols is increased. Thus, by choosing a suitable power level for the pilot symbols, the bit-error rate can be decreased.

Chapter 3

Estimators

In OFDM systems the optimal linear estimator in the mean-squared error sense is a 2-D (both time and frequency) filter. However, the complexity of this estimator is usually too large for it to be of practical use. A number of suboptimal low-complexity channel estimators have been suggested in the literature, see *e.g.*, [7, 20]. We will investigate two classes of estimators: 2-dimensional and separable. The use of separable filters is a common method to reduce complexity in multidimensional signal processing [21]. For both separable and non-separable estimators we look at FIR Wiener filters and low-rank approximations of LMMSE estimators. We compare all estimators' performances for two levels of complexity. Since they are all linear estimators, a reasonable measure of complexity is the average number of multiplications per estimated attenuation.

In the sequel we use the following notation. The backrotated, or least–squares-estimated, channel attenuations at pilot positions are denoted by

$$p_{k,l} = \frac{y_{k,l}}{x_{k,l}},$$

where $y_{k,l}$ is the received signal at subcarrier k in OFDM symbol l and $x_{k,l}$ is the corresponding transmitted pilot symbol. The final estimate of the channel attenuations $h_{k,l}$ are linear combinations of the $p_{k,l}$'s, where the coefficients are chosen according to each estimator's structure. By arranging the available LS estimates at pilot positions in a vector $\mathbf{p}$ and the channel attenuations to be estimated in a vector $\mathbf{h}$, the minimum mean-squared error estimator of $\mathbf{h}$ is [9]

$$\widehat{\mathbf{h}} = \mathbf{R}_{\mathbf{hp}}\mathbf{R}_{\mathbf{pp}}^{-1}\mathbf{p}, \tag{3.1}$$

where $\mathbf{R}_{\mathbf{hp}}$ is the cross-covariance matrix between $\mathbf{h}$ and $\mathbf{p}$, and $\mathbf{R}_{\mathbf{pp}}$ is the auto-covariance matrix of $\mathbf{p}$. Depending on the number of pilots used and their relative locations, the size of $\mathbf{p}$ and the corresponding auto-covariance matrix $\mathbf{R}_{\mathbf{pp}}$ will change. Also, depending on the number of estimated attenuations the size of $\mathbf{h}$ will change. Furthermore, $\mathbf{R}_{\mathbf{hp}}$ depends on the relative positions between estimated attenuations and the used pilot positions. Below we address several choices on used pilots and estimated attenuations.

3.1 2-D filters

The 2-D Wiener filter is optimal in terms of MSE, if complexity is not considered. However, for a fixed complexity, the number of filter taps that can be used is quite small. We use this estimator as a reference and investigate a reduced complexity estimator, which is derived using the theory of optimal rank-reduction [9].

3.1.1 2-D estimator

If the allowed complexity is K multiplications per attenuation, the two-dimensional filter uses the K pilots closest to the estimated attenuation. In Figure 3.1, we display an example of the seven pilot positions used ($K = 7$) to estimate one channel attenuation.

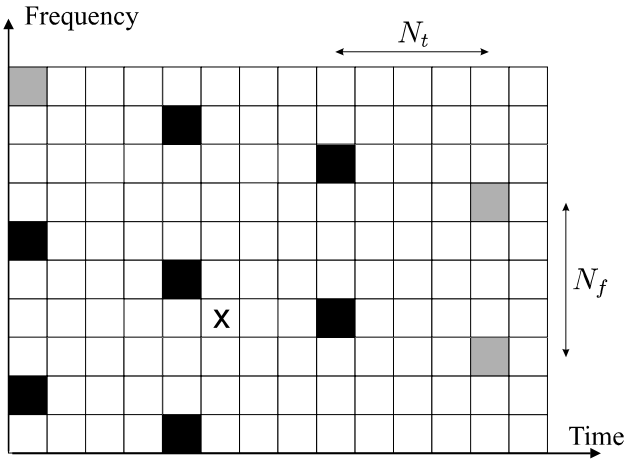

Figure 3.1: Two-dimensional FIR Wiener filter. The estimated tone (×) is a linear combination of the 7 pilot tones (■).

For every estimated channel attenuation there is a set of K associated pilots. Optimal weights are calculated according to (3.1). For the estimator with the lower complexity we will use the 3 closest pilots and for the higher complexity, the 13 closest.

3.1.2 Low–rank 2-D estimator

The low–rank 2-D estimator is in a sense an approximation of the optimal 2-D estimator in the previous section. The low complexity is achieved by a generalization of the ideas in [8]. To allow a low-rank approximation K_h attenuations, $\mathbf{h}$, are estimated simultaneously using the K_p closest pilots, $\mathbf{p}$. If the attenuations to be estimated and the pilots used are chosen properly, the estimator can be well approximated by a low-rank estimator, thereby reducing the complexity considerably while maintaining most of the performance. Note that the estimated attenuations can be chosen arbitrarily in the time-frequency grid. In Figure 3.2 an example is given for the location of estimated attenuations ($K_h = 15$) and the used pilot symbols ($K_p = 7$).

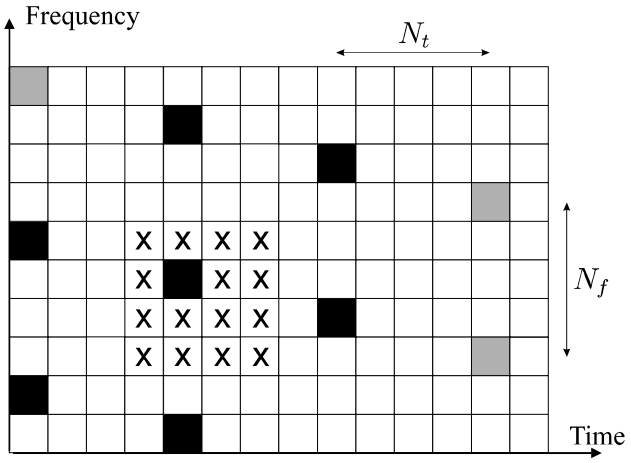

Figure 3.2: Structure of the low–rank 2-dimensional estimator. The tones to estimate are marked with (×) and the pilots used are marked with (■).

The estimator becomes

$$\widehat{\mathbf{h}} = \mathbf{G}_r \mathbf{p},$$

where $\mathbf{G}_r$ is a low-rank Wiener filter [9]. From the singular value decomposition (SVD)

$$\mathbf{R_{hp}} \mathbf{R_{pp}}^{-1/2} = \mathbf{U} \mathbf{\Sigma} \mathbf{V}^H,$$

where $\mathbf{U}$ and $\mathbf{V}$ are unitary matrices and $\mathbf{\Sigma}$ is a diagonal matrix [22], the low-rank Wiener filter is determined by [9]

$$\mathbf{G}_r = \mathbf{U} \mathbf{\Sigma}_r \mathbf{V}^H \mathbf{R_{pp}}^{-1/2},$$

where $\mathbf{\Sigma}_r$ is a $K_h \times K_p$ diagonal matrix containing the r largest singular values. The complexity of this estimator is found in Appendix A to be

$$r \left(1 + \frac{K_p}{K_h} \right) \tag{3.2}$$

multiplications per estimated attenuation, where r is the rank of the estimator (number of singular values used), K_p the number of pilots used and K_h the number of attenuations to be estimated.

For the lower complexity estimator we chose $K_p = 33$ pilots (3 in the time direction and 11 in the frequency direction) and $K_h = 64$ attenuations to estimate (4 in the time direction and 16 in the frequency direction). The latter were placed in the middle of the former in order to exploit as much correlation as possible. With a rank of $r = 2$, the number of multiplications per attenuation is, according to Eq. (3.2),

$$C_{\text{low}} = 2 \left(1 + \frac{33}{64} \right) = 3.0.$$

For the higher complexity we chose 80 pilots (4 in the time direction and 20 in the frequency direction) and 64 attenuations to estimate (4 in the time direction and 16 in

the frequency direction). The rank used was 6, giving

$$C_{\text{high}} = 6\left(1 + \frac{80}{64}\right) = 13.5.$$

multiplications per attenuation.

3.2 Separable filters

Since 2-D filters in general tend to have a large computational complexity, the outer product of two 1-D filters can give a good trade-off between performance and complexity. This is a standard technique in multidimensional signal processing [21] and it has also been proposed for pilot-based channel estimation in OFDM systems [7]. In pilot-based estimation schemes, the major advantage is the low number of multiplications per used pilot. This allows the estimator to be based on more pilots, thus improving the performance.

Based on the pilot pattern chosen, the general concept used in this report is shown in Figure 3.3, where a 1-D filter is applied in the frequency direction. Thereafter, a 1-D filter is applied in the time direction to complete the interpolation to all points in the grid.

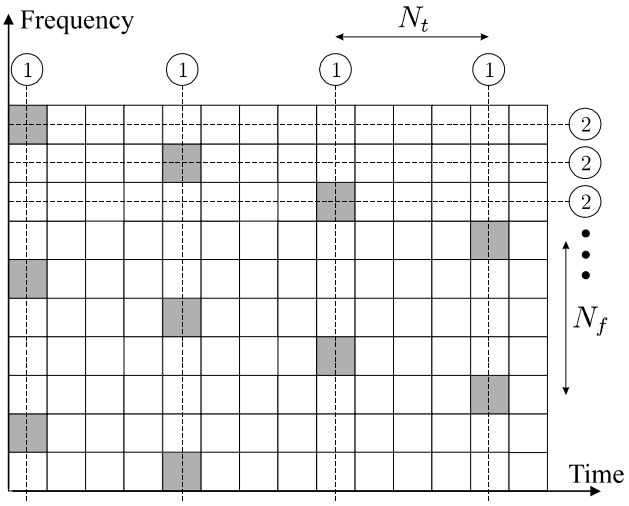

Figure 3.3: Separable filter based on one-dimensional filters in frequency (1) and time (2) directions. Filtering in the frequency direction (1) is performed first.

We investigate both an estimator based on the proposal in [7] and a variant thereof, which allows the use of more pilots by a low-rank approximation in the frequency direction.

3.2.1 Separable FIR filters

The use of separate 1-D FIR filters in the time and frequency directions has been proposed by Höher in [7]. First, all attenuations in OFDM symbols containing pilots are estimated.

This is done with a FIR Wiener filter of length K_f. Two attenuations on different positions relative to the pilots will need different filters, so there will be N_f different filters for this estimation. Note that these filters are non-causal in the sense that they will use pilots on both sides of the estimated attenuation in order to exploit the closest pilots. After this procedure there will be estimates of all attenuations in every N_t^{th} OFDM symbol. FIR Wiener filters of length K_t are now used in the time direction to obtain estimates of all attenuations. Here there will be $N_t - 1$ different filters, depending on which attenuation is estimated. These filters can be noncausal, which will introduce a delay in the system. If this delay cannot be accepted, causal filters must be used.

The total number of multiplications per estimated attenuation is

$$\frac{K_f}{N_t} + K_t$$

since the frequency-direction filter has to be applied in only one out of every N_t OFDM symbols. This fact can be used in the design of the filters since the frequency-direction filter taps are cheaper in terms of complexity. By reducing the number of taps in the time direction filter by one, N_f taps can be added to the frequency direction filter without changing the total complexity.

For the lower complexity we used 5 taps in the frequency filter and 2 taps in the time filter. This results in

$$C_{\text{low}} = \frac{5}{4} + 2 = 3.25$$

multiplications per attenuation. For the higher complexity, 25 and 7 taps were used for the frequency and time filters, respectively. This means a complexity of

$$C_{\text{high}} = \frac{25}{4} + 7 = 13.25$$

multiplications per attenuation.

3.2.2 Low-rank separable filter

By using observations from [8], where low-rank approximations of channel estimators are presented, we replace one of the FIR filters in the estimator proposed by Höher. Instead of FIR Wiener filters in both directions, a low-rank approximation of the frequency direction LMMSE estimator is used in combination with the time direction FIR filter. Hence, a frequency direction filtering is performed for each OFDM symbol containing pilots. An obvious way of doing this filtering is to estimate all attenuations in an OFDM symbol using all pilots. However, when using all pilots, the complexity reduction is not so large that it can compete with a short FIR Wiener filter. The number of multiplications per attenuation is (see Appendix A)

$$r\left(1 + \frac{K_p}{K_h}\right),$$

where r is rank used, K_h and K_p are the number of attenuations to estimate and number of pilots used, respectively. Since pilots far away from the estimated attenuations are

weakly correlated, they do not contribute much to the estimate. By excluding them, the complexity goes down while the performance is almost the same. Hence, the OFDM symbol is partitioned into a number of sub-symbols, where the attenuations are estimated using only the K_p pilots closest to the sub-symbol consisting of K_h subcarriers [8]. In Figure 3.4, an example is shown for $K_h = 8$ channel attenuations and $K_p = 5$ pilots. Low-rank approximations can be done for the time-direction filtering as well, but in this report we have chosen to use an FIR filter instead.

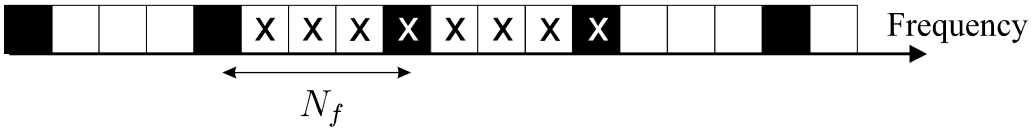

Figure 3.4: Structure of the low–rank estimator in the frequency direction. The $K_h = 8$ attenuations to estimate are marked with (×), and the $K_p = 5$ pilot symbols used are marked with (■).

We chose, for the lower complexity, to estimate 12 attenuations in the frequency direction using 7 pilots and a rank of 2. This results in $2\,(1 + 7/12) = 3.2$ multiplications per attenuation in the frequency direction. Combined with a 2-tap time filter, this gives a total of

$$C_{\text{low}} = \frac{3.2}{4} + 2 = 2.8$$

multiplications per attenuation. For the higher complexity we used 64 pilots to estimate 8 attenuations with a rank of 2. Together with a time filter with 9 taps, this gives

$$C_{\text{high}} = \frac{2\left(1 + \frac{64}{8}\right)}{4} + 9 = 13.\,5$$

multiplications per attenuation.

The four investigated estimators are summarized in Table 3.1.

Estimator	**Structure**	**# mult./att.**	**# pilots**
2-D	Uses the K_p closest pilots	K_p	K_p
Low-rank 2-D	Estimates K_h attenuations using K_p pilots and a rank of r	$r\left(1 + \frac{K_p}{K_h}\right)$	K_p
Separable	Separable FIR filter with K_f (frequency) and K_t (time) taps	$\frac{K_f}{N_t} + K_t$	$K_f K_t$
Low-rank separable	Estimates K_h attenuations using K_p pilots and a rank of r (frequency) and K_t taps FIR filter (time)	$\frac{r}{N_t}\left(1 + \frac{K_p}{K_h}\right) + K_t$	$K_p K_t$

Table 3.1: The four channel estimators investigated in this report.

3.3 Complexity and used pilots

Since all estimators are linear, the channel estimates are linear combinations of a number of pilots. The number of pilots used depends on the complexity and the type of estimator. The average number of multiplications per attenuation and the number of pilots the estimators are based on, are shown in Table 3.2. The estimators use the parameters described in the previous section. As can be seen in the table, for a fixed complexity the number of pilots used in the estimates can be increased by posing restrictions on the estimators, such as separability and low rank. However, because a large number of pilots are used, many will be only weakly correlated with the estimated channel attenuations and will not, therefore, contribute much. Thus, considering correlation mismatch in the design, the estimation may actually be degraded by increasing the number of used pilots. The main advantage of using many pilots is that the impact of the channel noise is reduced by a large averaging.

Estimator	**Low complexity**		**High complexity**	
	# mult./att.	# pilots	# mult./att.	# pilots
2-D	3	3	13	13
Low-rank 2-D	3.0	33	13.5	80
Separable FIR	3.25	10	13.25	175
Low-rank separable	2.8	14	13.5	576

Table 3.2: Average number of multiplications per tone and the number of pilots the estimators are based on.

3.4 Design aspects

In order to make the channel estimators attractive to implement, we assume that they are fixed, *i.e.,* designed for both a fixed channel correlation and a fixed SNR.

The frequency correlation is determined by the power delay profile of the channel [8] and the time correlation is determined by the Doppler frequency [17]. Neither the power delay profile, nor the Doppler frequency, are known by the receiver. Using our channel model we design the estimators for a maximum relative Doppler frequency of 5% and a uniform power-delay profile over the length of the cyclic prefix. The use of these worst case parameters follows the recommendations in [6], where pilot-symbol assisted modulation is analyzed. For the determination of the correlation matrices, see Appendix B. Contrary to the worst case recommendations for fixed design correlations, the fixed design SNR should be chosen to a best case. This implies a close to optimal performance for SNRs below the design SNR where the effects of SNR mismatch are small compared to the overall noise level. We have chosen the design SNR to 30 dB.

We evaluate the estimators under mismatch, *i.e.*, they are designed for the wrong channel correlation and SNR. Parameters for the design and the true values of the channel statistics are shown below in Table 3.3. Note that there is no mismatch in Doppler frequency. Given the design for 5 % relative Doppler frequency, the performance is

approximately the same for $f_{D,\max} \leq 5$ % [6]. The SNR is defined as the transmitted energy per data bit over the channel noise variance:

$$SNR \triangleq \frac{E\left\{|h_k|^2\right\} E\left\{|x_k|^2\right\}}{E\left\{|n_k|^2\right\}} \cdot \frac{1}{b},$$

where b denotes the number of information bits/symbol. In our case we have $b = 1$.

Parameter	**True**	**Design**
No. of subcarriers	1024	1024
Time dispersion	10 μs	10 μs
Power delay profile	$\begin{cases} Ce^{-\tau/2.2\mu s} & 0 < \tau < T_{cp} \\ 0 & \text{otherwise} \end{cases}$	$\begin{cases} 1/T_{cp} & 0 < \tau < T_{cp} \\ 0 & \text{otherwise} \end{cases}$
Max. rel. Doppler frequency	5%	5%
SNR	Varying	30 dB

Table 3.3: Design and true values of system parameters. The constant C is a normalization factor.

Chapter 4

Performance evaluation

We evaluate the performance of the four investigated estimators both in terms of mean-squared error (MSE) and coded bit-error rate (BER). The MSE is theoretically calculated while the BER is simulated. To simplify the MSE calculations, we ignore edge effects in the time-frequency grid and assume that it is of infinite extent. For a system where the number of subcarriers is much larger than the length of the estimator, these effects can be ignored.

4.1 Mean-squared error

Since all estimators are linear they can be expressed as

$$\widehat{\mathbf{h}} = \mathbf{G}\mathbf{p}$$

by collecting all used pilots in a vector $\mathbf{p}$ and calculating the corresponding estimator matrix $\mathbf{G}$. The covariance matrix of the error $\mathbf{e} = \mathbf{h} - \widehat{\mathbf{h}}$ can be expressed as [9]

$$\mathbf{R}_{\mathbf{ee}} = \mathbf{R}_{\mathbf{hh}} - \mathbf{R}_{\mathbf{hp}}\mathbf{G}^H - \mathbf{G}\mathbf{R}_{\mathbf{hp}}^H + \mathbf{G}\mathbf{R}_{\mathbf{pp}}\mathbf{G}^H. \tag{4.1}$$

For all estimators there will be different mean-squared errors depending on the estimated attenuation. In order to compare the estimators, we only look at the average error over all attenuations, *i.e.*

$$\text{MSE} = \frac{1}{K_h}\sum_{n=1}^{K_h}\mathbf{R}_{\mathbf{ee}}(n,n) = \frac{1}{K_h}\text{tr}\left(\mathbf{R}_{\mathbf{ee}}\right),$$

where K_h is the number of estimated attenuations and 'tr' denotes the trace of a matrix [22].

In Figure 4.1 the MSE for the estimators with the lower complexity level are shown as a function of SNR. It should be noted that the non-separable estimators have an error floor that is already visible at low SNR. For the separable estimators the error curves level out for very high SNRs, but this error floor is hardly noticeable in the figure. Because there will always be an interpolation error, even in the noiseless case, all the estimators

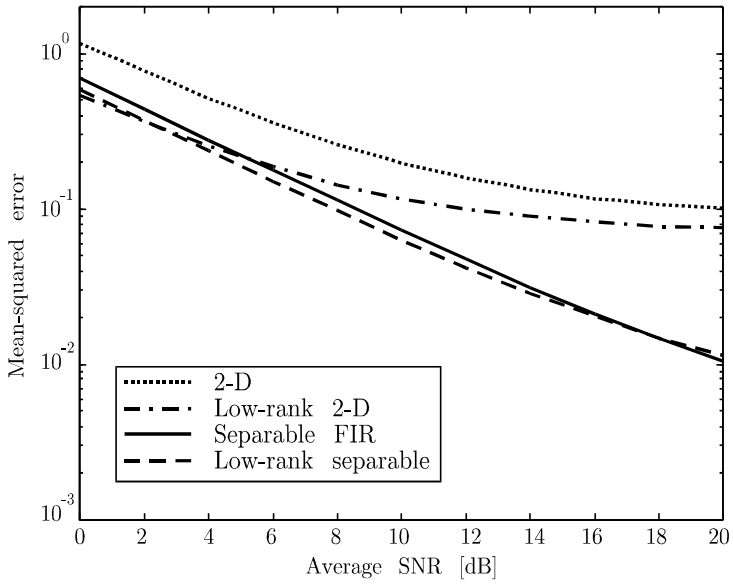

Figure 4.1: Mean-squared error (relative to channel power) for the four analysed estimators with the lower complexity (3 multiplications per tone).

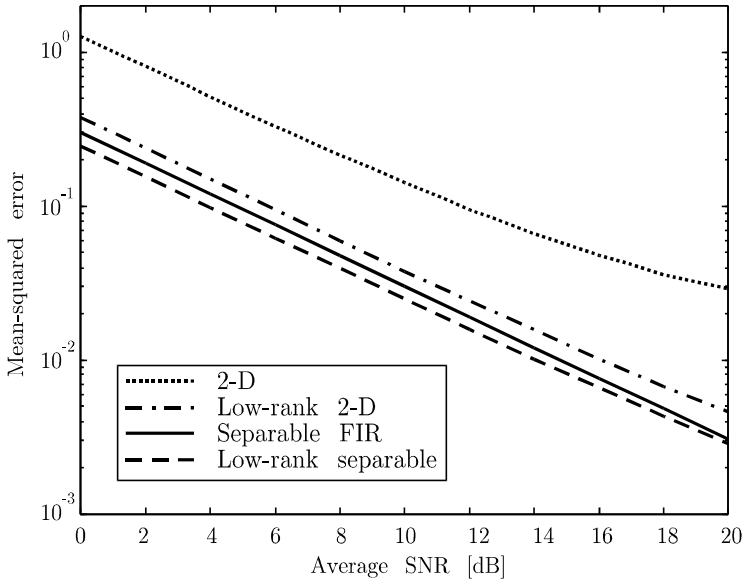

Figure 4.2: Mean-squared error (relative to the channel power) for the four analysed estimators with the higher complexity (13 multiplications per tone).

have an error floor. This is due to finite filter lengths. For SNR < 12 dB, the low-rank separable estimator is 0.7 dB better than separable FIR filters.

The MSE-curves for the higher complexity are shown in Figure 4.2. The error floors have now been lowered and are only noticeable for the 2-D estimator. Note also that the mutual ordering is the same as for the lower complexity, *i.e.* the low-rank separable estimator is the best and the 2-D estimator is the worst. The difference between the low-rank separable estimator and separable FIR filters is now about 0.8 dB. In both Figures. 4.1 and 4.2 it can be seen that separable estimators perform better than non-separable. This was noted in [7], where it was argued that separable estimators provide a good trade-off between complexity and performance.

4.2 Bit-error rate

The estimators have been simulated in the coded system. In Figure 4.3 the coded BER is shown for the estimators with the lower complexity ($\approx$3 multiplications per attenuation). As a reference, a system with perfect knowledge of the channel at the receiver is included. As observed above, all estimators suffer from an error floor, which appears due to the interpolation. In Figure 4.3 this is only noticeable for the 2-D estimator. The other estimators do not have this drawback for SNR < 10 dB and they perform better. It is also noticeable that estimators that perform well in terms of MSE also have a low BER, which is expected. The best estimator is the low-rank separable estimator, which is only about 1.4 dB worse than known channel and 0.2 dB better than separable FIR filters. Note that for MSE, this latter difference was 0.7 dB.

In Figure 4.4, the BER curves for the estimators with the higher complexity are shown. Again, the BER with known channel is included as a reference.

The low-rank separable estimator is now only 0.7 dB away from known channel and still about 0.2 dB better than separable FIR filters. In this figure we note that the performance of all estimators has increased, but the ordering between them is not changed, *i.e.,* the low-rank separable estimator is the best and the 2-D is the worst. The investigation here suggests that this holds for most complexity levels. However, for other types of channels and scenarios (such as the uplink), another estimator might be better. Separate studies are required for these circumstances.

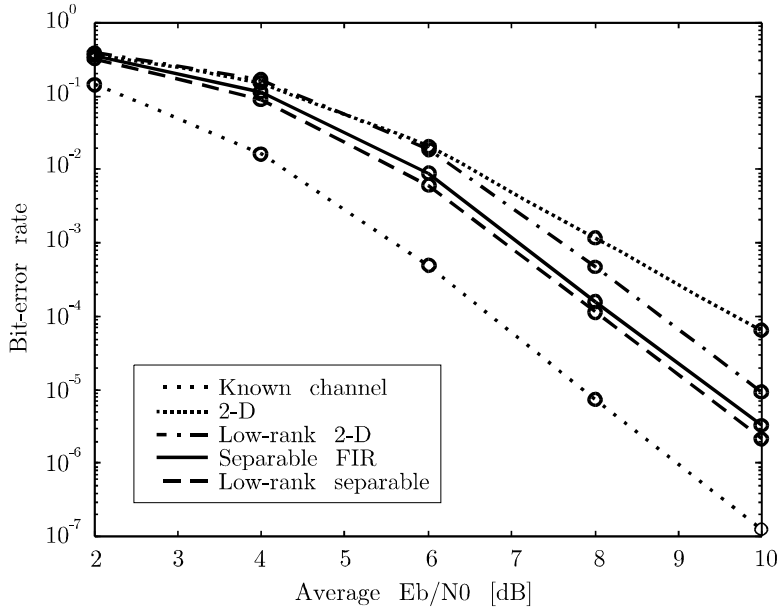

Figure 4.3: Coded bit-error rate with the low-complexity estimators.

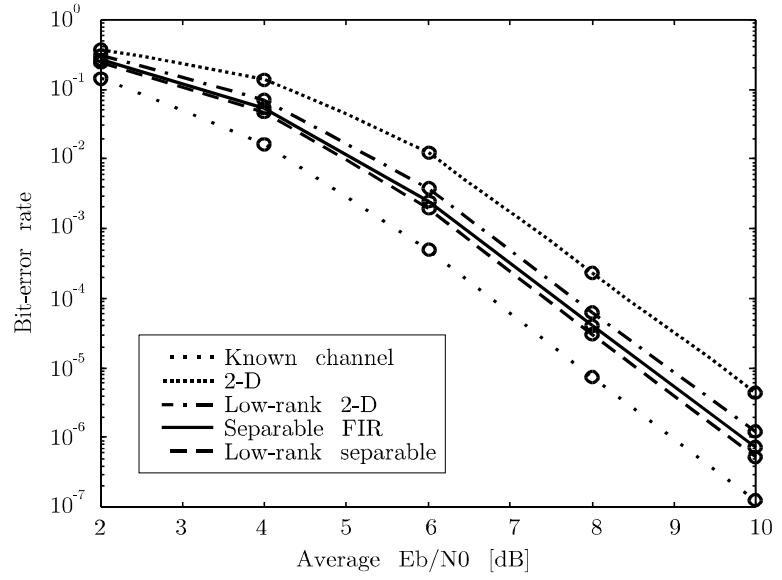

Figure 4.4: Coded bit-error rate with the high-complexity estimators.

Finally, the two levels of complexity for the low-rank separable estimator (which was shown to be the best) are compared to known channel. In Figure 4.5 it can be seen that the low and high complexity estimators are about 1.4 dB and 0.7 dB away from known channel, respectively. The BER will decrease with increasing complexity, but to get really close to the performance of known channel, a very high complexity is needed. This prompts an analysis of the trade-off between complexity and performance, but this is beyond the scope of this report.

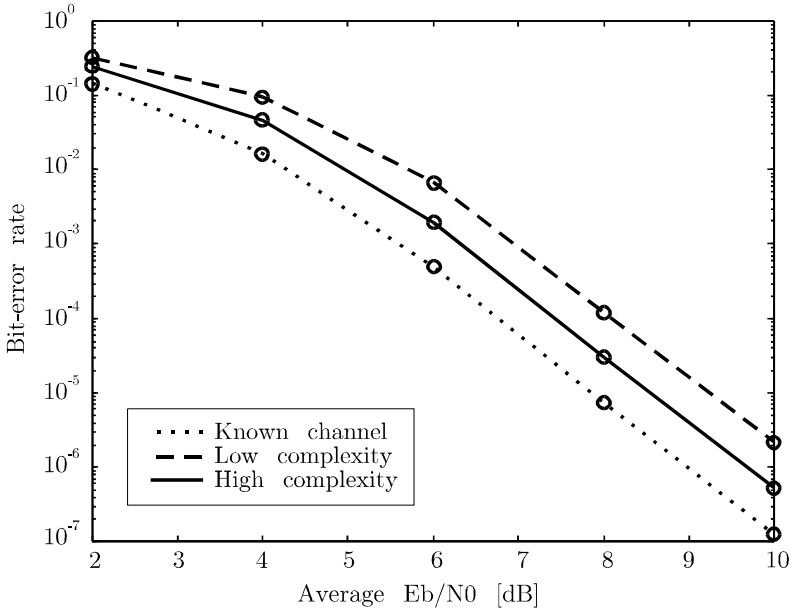

Figure 4.5: BER of known channel and the separable low-rank estimator of low complexity (3 mult./att.) and high complexity (13 mult./att.).

Chapter 5

Conclusions

In this report we have investigated four OFDM channel estimators suitable for broadcasting or for the downlink in a multiuser system. The estimators use pilots, *i.e.*, known symbols transmitted in certain positions in the time-frequency grid of OFDM. Two classes of estimators, 2-dimensional and separable, were investigated. Within each class we compared an FIR Wiener filter with a low-rank LMMSE estimator. Through analytical calculations of the MSE and simulation of the coded BER, it was found that the separable estimators were the best for a fixed complexity. Within the class of separable estimators, the low-rank estimator was shown to be about 0.2 dB better than the FIR estimator for the coded BER. Two levels of complexities were investigated, 3 and 13 multiplications per estimated attenuation, and it was found that for the coded BER, the former is 1.4 dB from known channel and the latter 0.7 dB. A natural continuation of this investigation of channel estimation in OFDM systems is a more comprehensive study of the trade-off between complexity and performance.

We have used a pilot pattern where 6% of the transmitted symbols are known. This pilot pattern is sufficient to obtain good estimations of the channel attenuations, while introducing only a small overhead. We have assumed that the receiver can use all pilot symbols that are transmitted. Generally, this is not the case in the uplink in a multiuser system, where the channel estimation can be based only on pilots transmitted by a single user. Hence, for the uplink a separate study must be made to investigate the performance of the channel estimators.

Appendix A

Complexity of low-rank estimators

The low-rank 2-D estimator can be formulated as

$$\widehat{\mathbf{h}} = \mathbf{G}_r \mathbf{p} = \sum_{k=1}^{r} \mathbf{g}_k \mathbf{g}_k^H \mathbf{p} = \sum_{k=1}^{r} \langle \mathbf{g}_k, \mathbf{p} \rangle \, \mathbf{g}_k,$$

since $\mathbf{G}_r$ is a rank-r matrix. The inner products $\langle \mathbf{g}_k, \mathbf{p} \rangle$ require K_p multiplications each, *i.e.* a total of rK_p multiplications. The linear combination is over r vectors of length K_h, *i.e.* requires rK_h multiplications. Since K_h attenuations are simultaneously estimated, the number of multiplications per attenuation becomes

$$\frac{rK_p + rK_h}{K_h} = r\left(1 + \frac{K_p}{K_h}\right).$$

Appendix B

Correlation matrices

The auto-correlation of the channel model (2.2) is

$$\begin{aligned} R_{GG}(\Delta f, \Delta t) &= E\left\{G(f;t)\, G^*(f-\Delta f; t-\Delta t)\right\} \\ &= E\left\{\frac{1}{M}\sum_{n,n'=1}^{M} e^{j(\theta_n-\theta_{n'})} e^{j2\pi\left(F_{D,n}t - F_{D,n'}(t-\Delta t)\right)} e^{-j2\pi(f\tau_n-(f-\Delta f)\tau_{n'})}\right\}. \end{aligned}$$

Since all random variables are independent, we have

$$\begin{aligned} R_{GG}(\Delta f, \Delta t) &= \frac{1}{M}\sum_{n=1}^{M} E\left\{e^{j2\pi F_{D,n}\Delta t}\right\} E\left\{e^{-j2\pi\Delta f\tau_n}\right\} \\ &= E\left\{e^{j2\pi F_{D,n}\Delta t}\right\} E\left\{e^{-j2\pi\Delta f\tau_n}\right\} = R_f(\Delta f)\, R_t(\Delta t), \end{aligned}$$

i.e., the channel correlation is separable. The expectations can be found from standard Fourier transforms [23]

$$\begin{aligned} R_t(\Delta t) &= E\left\{e^{j2\pi F_{D,n}\Delta t}\right\} = J_0(2\pi F_{D,\max}\Delta t) \\ R_f(\Delta f) &= E\left\{e^{-j2\pi\Delta f\tau_n}\right\} = \frac{\left(1-e^{-T_{cp}(1/\tau_{\mathrm{rms}}+j2\pi\Delta f)}\right)}{\left(1-e^{-T_{cp}/\tau_{\mathrm{rms}}}\right)(1+j2\pi\Delta f\tau_{\mathrm{rms}})}, \end{aligned}$$

where $J_0(\cdot)$ is the zeroth order Bessel function of the first kind. Note that the correlation function for the uniform power-delay profile can be obtained by letting $\tau_{\mathrm{rms}} \to \infty$:

$$R_f^{\mathrm{uniform}}(\Delta f) = \frac{1-e^{-j2\pi\Delta f T_{cp}}}{j2\pi\Delta f T_{cp}}.$$

The correlation between channel attenuations separated by k subcarriers and l OFDM symbols is

$$E\left\{h_{k',l'}h^*_{k'-k,l'-l}\right\} = r_f(k)\, r_l(l),$$

where

$$\begin{aligned} r_f(k) &= R_f\left(\frac{k}{NT_s}\right) = \frac{\left(1-e^{-L(1/\widetilde{\tau}_{\mathrm{rms}}+j2\pi k/N)}\right)}{\left(1-e^{-L/\widetilde{\tau}_{\mathrm{rms}}}\right)(1+j2\pi k\widetilde{\tau}_{\mathrm{rms}}/N)} \\ r_t(l) &= R_t(l(N+L)T_s) = J_0\left(2\pi f_{D,\max}\left(1+\frac{L}{N}\right)l\right), \end{aligned}$$

and $\widetilde{\tau}_{\mathrm{rms}} = \tau_{\mathrm{rms}}/T_s$ is the RMS-spread relative to the sampling interval. Since the LS-estimates at pilot positions are

$$p_{k,l} = \frac{y_{k,l}}{x_{k,l}} = h_{k,l} + \frac{n_{k,l}}{x_{k,l}},$$

the cross-correlation and the auto-correlation are

$$\begin{aligned} E\left\{h_{k,l}p^*_{k',l'}\right\} &= r_f\left(k-k'\right) r_t\left(l-l'\right) \\ E\left\{p_{k,l}p^*_{k',l'}\right\} &= r_f\left(k-k'\right) r_t\left(l-l'\right) + \sigma_n^2 E\left\{\frac{1}{\left|x_k\right|^2}\right\} \delta\left(k-k', l-l'\right). \end{aligned}$$

Using these functions, the auto-correlation $\mathbf{R}_{pp}$ and the cross-correlation $\mathbf{R}_{hp}$ can be calculated.

Bibliography

[1] Radio broadcasting systems; Digital Audio Broadcasting (DAB) to mobile, portable and fixed receivers. ETS 300 401, ETSI – European Telecommunications Standards Institute, Valbonne, France, February 1995.

[2] Tristan de Couasnon, Raoul Monnier, and Jean Bernard Rault. OFDM for digital TV broadcasting. *Signal Proc.*, 39(1–2):1–32, September 1994.

[3] Digital broadcasting systems for television, sound and data services. European Telecommunications Standard, prETS 300 744 (Draft, version 0.0.3), April 1996.

[4] Volker Engels and Hermann Rohling. Multilevel differential modulation techniques (64-DAPSK) for multicarrier transmission systems. *Eur. Trans. Telecommun. Rel. Technol.*, 6(6):633–640, November 1995.

[5] Michael L. Moher and John H. Lodge. TCMP – A modulation and coding strategy for Rician-fading channels. *IEEE J. Select. Areas Commun.*, 7(9):1347–1355, December 1989.

[6] James K. Cavers. An analysis of pilot-symbol assisted modulation for Rayleigh-fading channels. *IEEE Trans. Vehic. Technol.*, 40(4):686–693, November 1991.

[7] Peter Höher. TCM on frequency-selective land-mobile fading channels. In *Proc. Tirrenia Int. Workshop Digital Commun.*, Tirrenia, Italy, September 1991.

[8] Ove Edfors, Magnus Sandell, Jan-Jaap van de Beek, Sarah Kate Wilson, and Per Ola Börjesson. OFDM channel estimation by singular value decomposition. Research Report TULEA 1996:18, Div. of Signal Processing, Luleå University of Technology, September 1996.

[9] Louis L. Scharf. *Statistical signal processing: Detection, estimation, and time series analysis.* Addison-Wesley, 1991.

[10] A. Peled and A. Ruiz. Frequency domain data transmission using reduced computational complexity algorithms. In *Proc. IEEE Int. Conf. Acoust., Speech, Signal Processing*, pages 964–967, Denver, CO, 1980.

[11] S. B. Weinstein and Paul M. Ebert. Data transmission by frequency-division multiplexing using the discrete Fourier transform. *IEEE Trans. Commun.*, COM-19(5):628–634, October 1971.

[12] John A. C. Bingham. Multicarrier modulation for data transmission: An idea whose time has come. *IEEE Commun. Mag.*, 28(5):5–14, May 1990.

[13] A. Müller. OFDM transmission over time-variant channels. In *Proc. Int. Broadc. Conv.*, number 397, pages 533–538, Amsterdam, Netherlands, September 1994.

[14] Mark Russell and Gordon Stüber. Interchannel interference analysis of OFDM in a mobile environment. In *Proc. IEEE Vehic. Technol. Conf.*, volume 2, pages 820–824, Chicago, IL, July 1995.

[15] Stephen G. Wilson. *Digital modulation and coding*. Prentice-Hall, New Jersey, USA, 1996.

[16] Peter Höher. A statistical discrete-time model for the WSSUS multipath channel. *IEEE Trans. Commun.*, 41(4):461–468, November 1992.

[17] William C. Jakes. *Microwave mobile communications*. Classic Reissue. IEEE Press, Piscataway, New Jersey, 1974.

[18] J.G. Proakis. *Digital communications*. Prentice-Hall, 3rd edition, 1995.

[19] A.V. Oppenheim and R.V. Schafer. *Discrete-time signal processing*. Prentice-Hall, 1989.

[20] Gordon L. Stüber and Mark Russell. Terrestrial digital video broadcasting for mobile reception using OFDM. In *Proc. Globecom*, volume 3, pages 2049–2053, Singapore, November 1995.

[21] Dan E. Dudgeon and Russell M. Mersereau. *Multidimensional digital signal processing*. Prentice–Hall, Englewood Cliffs, NJ, 1984.

[22] G.H. Golub and C.F. van Loan. *Matrix Computations*. North Oxford Academic, Johns Hopkins Academic Press, 2nd edition, 1989.

[23] M. Abramovitz and I.A. Stegun. *Handbook of mathematical functions with formulas, graphs and mathematical tables*. Number 55 in Applied Math. Series. Nat. Bureau of Stand., Washington, DC, USA, 1964.